2023 19th International Symposium on Medical Information Processing and Analysis (SIPAIM) | 979-8-3503-2523-2/23/$31.00 ©2023 IEEE | DOI: 10.1109/SIPAIM56729.2023.10373540

Along-Tract Parameterization of White Matter Microstructure using Medial Tractography Analysis (MeTA)

Iyad Ba Gari[1], Shayan Javid[1], Alyssa H. Zhu[1], Shruti P. Gadewar[1], Siddharth Narula[1], Abhinaav Ramesh[1], Sophia I. Thomopoulos[1], Lachlan Strike[2], Greig I. de Zubicaray[3], Katie L. McMahon[3], Margaret J. Wright[4], Paul M. Thompson[1], Talia M. Nir[1], Neda Jahanshad[1], for the Alzheimer's Disease Neuroimaging Initiative

[1]*Imaging Genetics Center, Mark and Mary Stevens Neuroimaging and Informatics Institute, Keck School of Medicine of USC, University of Southern California, Marina del Rey, CA*

[2]*QIMR Berghofer Medical Research Institute, Brisbane, QLD, Australia*

[3]*Queensland University of Technology, Brisbane, QLD, Australia*

[4]*Queensland Brain Institute, University of Queensland, Brisbane, QLD, Australia*

bagari@usc.edu & njahansh@usc.edu

***Abstract*— Diffusion MRI tractography is a noninvasive method to estimate the structural connectivity of white matter (WM) bundles (tracts) in the human brain, which can help us understand brain function and neurodegenerative diseases. Existing techniques for analyzing WM microstructure along the length of bundles often require registering all individuals into a common space that may ignore potentially key differences in the shape and alignment of the tracts. We propose the Medial Tractography Analysis (MeTA) method to reduce partial voluming and microstructural heterogeneity in dMRI metrics while retaining bundle shape and capturing the regional variation within bundles. We performed reliability, compatibility, and disease-based validations. MeTA showed moderate to good overall overlap for most bundles in a test-retest dataset and preserved regional compatibility when applied to a dataset of subjects scanned with both high and low angular resolution protocols. Diffusion tensor imaging (DTI) metrics along the length of MeTA bundles had strong associations with cognitive impairment in ADNI. MeTA may be a reliable approach to identify regional abnormalities in clinical populations across multiple diffusion acquisitions.**

Keywords—Diffusion MRI, tractography, white matter bundle, medial volume, along-tract analysis

I. Introduction

Diffusion-weighted magnetic resonance imaging (dMRI) is a noninvasive technique that can be used to visualize the white matter (WM) in the brain and quantify its microstructural properties. Whole brain "tractograms" can be generated and segmented into specific WM tracts or pathways, to study and reveal normal variations and abnormal alterations with disease progression [1].

Tracts may vary spatially along their length with different segments being more susceptible to disease. To chart localized variations, methods for performing population-based analyses of microstructural WM along the bundle have been established. One method uses cubic B-splines to reparameterize the streamlines of the bundle into N (100) points equally spaced along their length [2] and maps them onto a single curve. Then, the average of diffusion tensor imaging (DTI) metrics are output for each point along the tract instead of a single scalar value across the entire tract. Another method uses QuickBundles [3] to generate a centroid with 100 points [4] segmented in a common space and determines correspondence between subjects using a distance metric. The first method is agnostic to shape differences between subjects, while the second is dependent upon registration to a common space. Full streamline based analyses are computationally intensive when large numbers of streamlines are generated and may require registering streamlines across subjects into a common space for group analysis [5].

We have developed a novel method, Medial Tractography Analysis (MeTA), that aims to reduce microstructural heterogeneity and variability of dMRI metrics within bundles, and take into account correspondence of regional along-tract comparisons between subjects across acquisition protocols, by focusing on the core of the bundle. MeTA builds on tract segmentation tools to extract the core *volume* of the bundle instead of the medial surface [6]–[8]. We propose a framework for expanding MeTA by segmenting the core WM tracts along the curve and establishing correspondence across subjects in their native spaces, even when bundles across subjects have different lengths and shapes. This process does not require all subjects' data to be registered into a common space, which can be computationally expensive and prone to misregistrations. We used test-retest data from the WU-Minn Human Connectome Project (HCP), a compatibility dataset from the Queensland Twin IMaging (QTIM) study, and clinical multi-protocol dataset from the Alzheimer's Disease Neuroimaging Initiative (ADNI3) to validate our method [9]–[11]. We show that we can extract reliable DTI metrics across different segments, that our MeTA-based along-tract regional estimates are more compatible than full bundle analytics. We found that we could detect more robust associations with clinical measures than using the full bundle, all in native space, without computationally intensive bundle-level non-linear registration.

II. Methods

A. Medial Surface and Core Extraction

A continuous medial representation (CM-Rep) **m** is a parametrized surface model with a radius scalar field (**R**) attached to the surface [7]. To reconstruct the boundary of a 3D object **X**, a maximum inscribed ball (MIB) of radius **R** is placed on each point of the continuous medial surface (**m**). The object **X** can be described as $\mathbf{X}^{\pm}(u)$, where X^+ and X^- are on opposite sides of a parametrized surface **m**(u), where u is a

surface parameter of m. The points of tangency between X and the MIB of m with radius R can be considered as $X^{\pm}$.

$$X^{\pm}(u) = m(u) + R(u)\,U^{\pm}(u) \quad (1)$$

The unit outward normal vectors on both directions of X are denoted by $U^{\pm}$ in the equation.

$$U^{\pm} = -\nabla_m R \pm \sqrt{1 - \|\nabla_m R\|^2}\, N_m \quad (2)$$

where N_m denotes the unit normal to the medial surface (m) and $\nabla_m R$ is the Riemannian gradient of R on m.

To compute the central 25% 'core' of the 3D volumetric shape, we used the medial surface (m) and boundary mesh X [6]. This involved computing the 37.5% and 62.5% surfaces using ray tracing methods (12.5% around the medial 50% surface) [12]. We determined the normal on the vertex points of the medial surface (m) and traveled along the surface normal in both directions $X^{\pm}$ to reach the outer boundary mesh points. We refer to this as the MeTA_25% 'core'.

We used a KD-Tree [13] to determine the distance between each individual vertex point on the medial surface m and its nearest vertex point on the outer boundary mesh $X^{\pm}$, taking into account the normal axis in both directions. By doing so, we were able to calculate the shortest distance (thickness/depth) from the vertex point on the medial surface to the boundary mesh. The newly computed points on both sides of the medial surface were used to obtain the sub-volume from the original boundary.

B. Bundle Core Parcellation

To achieve correspondence between subjects, we generated a centroid along the length of the template bundle with 14 points to get 15 segments along the length of the bundle, where 15 was chosen arbitrarily as the number of segments, which serves as a reference for comparison across subjects [14]. We generated the subject's centroid for each bundle with 100 points using QuickBundles [3] and used dynamic time warping (DTW) to get the corresponding points between the subject and template bundles, as shown in **Figure 1**. Given two sequences of possibly different lengths, DTW calculates the optimal correspondence between the two sets of points by minimizing the Euclidean distance between the two sequences under all possible sets of alignments [15]. DTW will match each point in the model's centroid with more than one point in the subject's centroid, and we therefore pick the midpoint of all possible matches and return the corresponding 14 points in the subject's centroid that will be used in the parcellation of MeTA_25% 'core'.

Using the subject centroid points, we divided the full 3D binary mask of the bundle ('all') into multiple segments, as illustrated in **Figure 1**. We assigned each voxel of the entire bundle to the appropriate segment based on its relative position to the DTW points, as determined by using dot product calculations between a vector of two consecutive corresponding points and a vector of the current corresponding point and all other points. For ambiguous voxels with unassigned or multiply assigned segments, we reassigned these voxels by identifying the segment whose DTW point is closest according to the Euclidean distance.

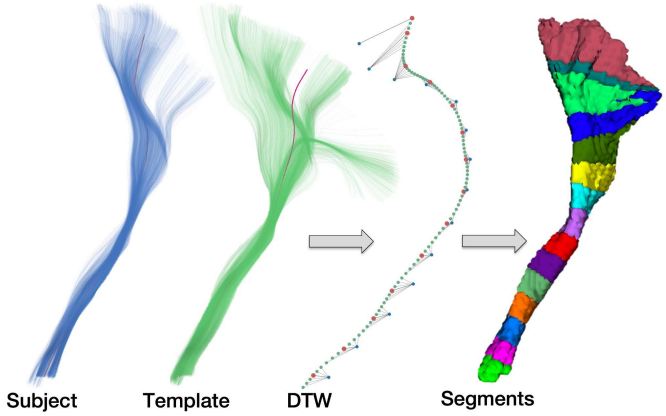

Fig. 1. **Bundle core parcellation workflow.** While the CM-rep surface is used for representing the bundles, the centroid curve is used for alignment. A centroid (in *red color*) is generated from the segmented bundle of the subject (in *blue color*) containing 100 points and the template bundle (in *green color*) with 14 points. DTW was used to get corresponding points by aligning these two centroids. The parcel bundle core volume was obtained by using corresponding points.

C. Datasets

In our reproducibility and compatibility analyses (**Table I**), we used test-retest data from the HCP and two acquisitions from the QTIM datasets, the latter of which comes in two protocols collected at 4 tesla: low and high angular resolution (LARDI and HARDI, respectively). We downloaded preprocessed dMRI data from the HCP. The QTIM datasets were previously corrected for eddy current and motion artifacts using FSL's eddy_correct, and then corrected for EPI distortion by registering to a downsampled version of the subject's T1-weighted image in MNI space; both protocols were resampled to $(2\text{mm})^3$ in the process. For our clinical application, we also applied our method to the ADNI3 dataset. The ADNI3 dataset was denoised using Local PCA [16], deGibbs [17], and corrected for eddy current and motion artifacts (using FSL eddy [18]).

TABLE I. DEMOGRAPHIC DETAILS FOR RELIABILITY AND COMPATIBILITY DATASETS.

Dataset	Age range	N (F)	Voxel size (mm^3)	N (Volume)	*b*-value (mm^2/s)
HCP	22-35	32 (23)	1.25 x 1.25 x 1.25	96, 96, 96 (90 non b0)	1000, 2000, 3000
QTIM (LARDI)	24-30	311 (189)	1.8 x 1.8 x 5	30 (27 non b0)	1146
QTIM (HARDI)			1.79 x 1.79 x 2	105 (94 non b0)	1159

We extracted the fiber orientation distributions (iFOD2) model for the whole brain using a multi-tissue constrained spherical deconvolution approach [19]. Then, we generated probabilistic streamlines tractography for the whole brain using the probabilistic iFOD2 method [20].

Using RecoBundles [8], which automatically groups streamlines into bundles using priors [14], major WM bundles were extracted from tractograms. Here, we focus on the arcuate fasciculus (AF), inferior fronto-occipital fasciculus

(IFOF), corticospinal tract (CST), all of which are bilateral and include both left and right sides, and the corpus callosum major (CC_ForcepsMajor). For each extracted bundle, we used CM-Rep to calculate the medial surface [7], and then extracted the MeTA_25% volume [6].

D. Reliability and Compatibility Statistics

First, we computed the Dice score for each of the four tracts (AF, IFOF, CST, CC_ForcepsMajor) as a general measure of volume similarity. The Dice overlap coefficient is a measure of the similarity between two datasets and is defined as two times the intersection of the two datasets divided by the sum of the volumes of each dataset. This was calculated in the fully segmented tract using RecoBundles ('all', i.e., 100%), MeTA_25% core and 15 segments along the length of core volume to determine the reproducibility of our parcellation workflow. Moreover, we calculated the intraclass correlation (ICC) of the FA measures using the psych library in R (https://cran.r-project.org/package=psych) to evaluate the test-retest reliability for HCP. We used the mean of k raters of ICC2 to eliminate the mean difference between scan sessions and take into account the random effect [21].

$$ICC2 = \frac{BMS - EMS}{BMS + (k-1)\,EMS + k\,(JMS - EMS)/n'} \quad (3)$$

where *BMS* stands for between-targets mean square (subjects), *EMS* is the residual mean square, *JMS* is the between-judges (scan sessions at HCP) mean square, k is the number of judges rating each target, and n' is the number of targets (subjects).

We evaluated the compatibility between the two different protocols (LARDI and HARDI) of the QTIM dataset using ICC3.

$$ICC3 = \frac{BMS - EMS}{BMS + (k-1)\,EMS} \quad (4)$$

E. Clinical Dataset Application

Using MeTA, we sought to find tracts and subregions associated with cognitive impairment. In ADNI3 (**Table II**), we evaluated the average DTI FA and MD bundle ('all', MeTA_25% 'core', and 15 MeTA_25% segments) associations with 1) clinical impairment in participants with mild cognitive impairment (MCI) or Alzheimer's disease (AD) compared to cognitively normal (CN) individuals; 2) Clinical Dementia Rating Scale Sum of Boxes (CDR-SB); and 3) tau positivity indexed with AV-1451 positron emission tomography in temporal lobe SUVRs [22]. In addition to the AF, IFOF, CST, and CC_ForcepsMajor, we evaluated the parahippocampal cingulum (C_PH), which is highly impacted in AD [11]. We applied RecoBundles [8] to segment the C_PH from the ADNI3 data. In linear mixed models, age and sex covariates were modeled as fixed effects, while protocol (**Table II**) was modeled as a random effect. We corrected for multiple comparisons across 153 tests: 9 bundles (AF_L, AF_R, CST_L, CST_R, IFOF_L, IFOF_R, CPH_L, CPH_R, CC_ForcepsMajor) and 17 regions (the bundle 'all', MeTA_25% 'core', and the 15 MeTA_25% segments) using the false discovery rate (FDR) procedure (q=0.05).

TABLE II. DEMOGRAPHIC AND CLINICAL MEASURES FOR PARTICIPANTS IN THE ADNI3 DATASET, SPLIT BY DMRI PROTOCOL.

Protocols	N (Female)	Age (yrs)	CN (MCI/AD)	tau$^-$ (tau$^+$)
P33	56 (22)	75.7±7.7	37 (19)	26 (11)
P36	46 (22)	73.1±6.9	20 (26)	22 (15)
S31	96 (57)	72.0±8.5	59 (37)	56 (21)
S55	262 (146)	74.5±7.9	170 (92)	138 (66)
S127	110 (59)	73.6±7.6	67 (43)	65 (21)
GE36	41 (18)	71.8±6.7	21 (20)	25 (9)
GE54	103 (50)	76.3±8.1	66 (37)	61 (22)
Total	714 (374)	74.1±7.9	440 (274)	393 (165)

III. RESULTS

A. Bundle Overlap, Microstructure Reliability and Compatibility

The results of the Dice overlap coefficient for the HCP dataset, including the full bundle ('all'), MeTA_25% ('core'), and 15 segments along MeTA_25% are shown in **Figure 2**. Most labels indicate moderate-to-good overall overlap for most bundles in the HCP dataset. The QTIM dataset in **Figure 3** shows a lower Dice score across the full bundle and MeTA_25% of all WM pathways. The beginning and ending of each bundle tend to have lower scores, while the middle segments have higher Dice scores. In QTIM, the CST segments 1 and 2 have a Dice score of zero due to the different fields of view between the HARDI and LARDI acquisition protocols. This may be expected given the large difference in slice thickness.

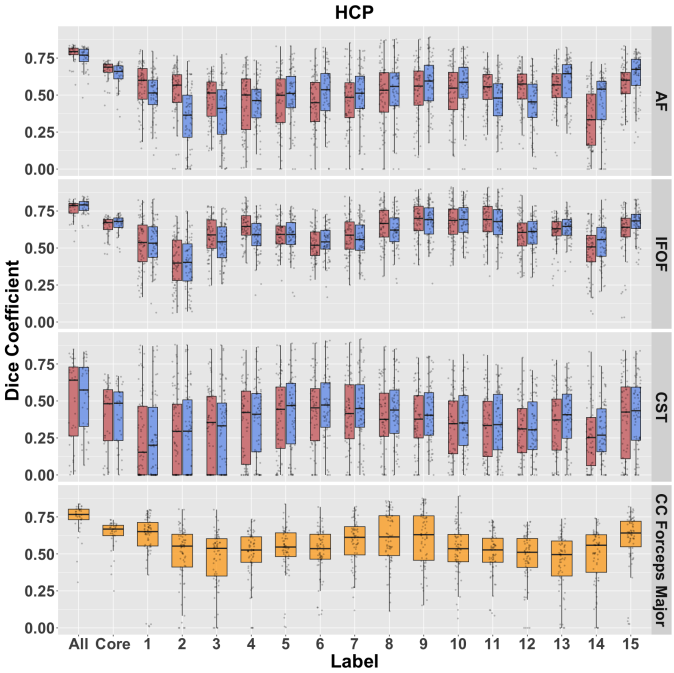

Fig 2. The Dice overlap coefficient for test-retest data from the HCP dataset is shown for bundles of (AF, IFOF, CST) across the left (in red) and right (in blue), as well as the Corpus Callosum Major tract (in yellow), for the full bundle ('all'), MeTA_25% ('core'), and 15 MeTA_25% segments.

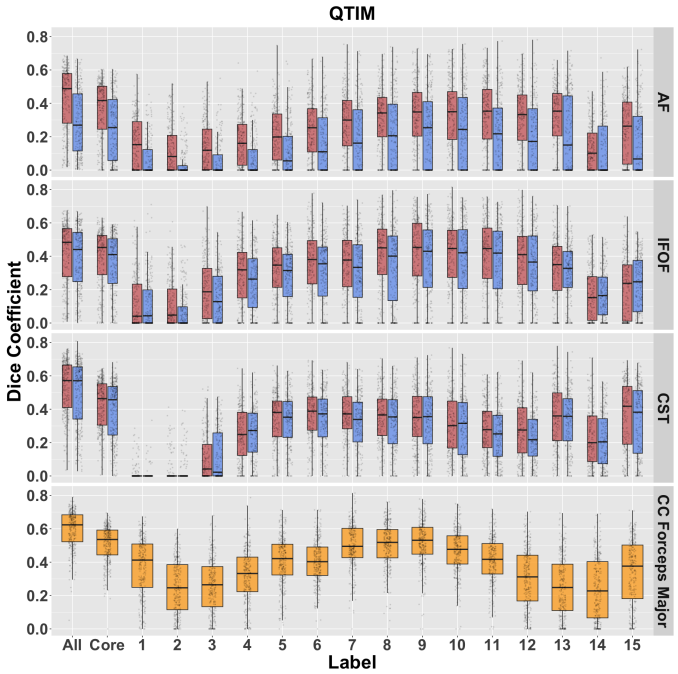

Fig 3. Dice scores for bundles of (AF, IFOF, CST) are shown on the left (in red) and right (in blue), as well as the Corpus Callosum Major tract (in yellow), for the full bundle ('all'), MeTA_25% ('core'), and 15 segments along MeTA_25% length across acquisition protocols of the QTIM dataset. *The local segments (1, 2) of the CST bundle have a zero dice score due to the different fields of view and slice thicknesses between the QTIM protocols.

Overall, the ICC of FA for the high-quality HCP dataset was moderate to highly reliable (ICC > 0.5) across all tracts for the full bundle ('all'), MeTA_25%, and most 15 segments along MeTA_25% length. In the QTIM dataset, moderate local compatibility was found in segments along MeTA_25% length. The ICC of the segments was often higher than that of the full bundle and was moderately compatible on several segments across all tracts across protocols. We note harmonization would improve compatibility.

TABLE III. MEAN FA ICC3K COMPATIBILITY ESTIMATES ACROSS 4 LATERALIZED TRACTS FOR ALL, CORE (META_25%) AND 15 SEGMENTS ALONG META_25% IN THE QTIM DATASET.

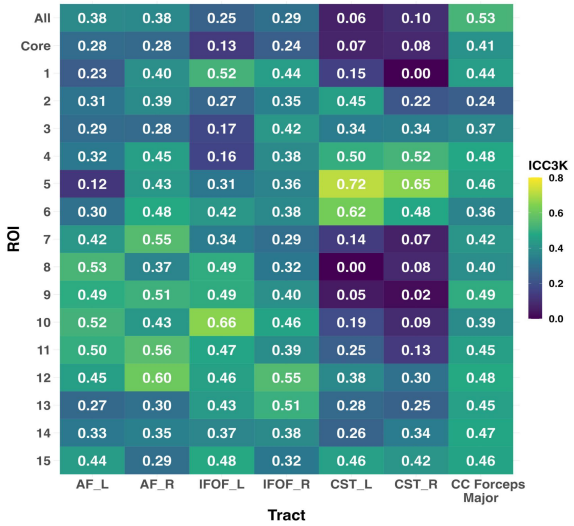

B. *ADNI Cognitive and Clinical Associations*

In general, participants with cognitive impairment, tau pathology, and higher CDR-SB scores showed negative associations with FA and positive associations with MD measure across all bundles, as expected. A subset of our regional results is displayed in **Figure 4**. Our analysis of DTI values in the MeTA_25% core volume and its segments showed some regional associations to be stronger than the full bundle ('all').

TABLE IV. DTI MEASURES IN THE LEFT ARCUATE FASCICULUS WERE SIGNIFICANTLY DIFFERENT ($*P_{FDR}<0.05$) BETWEEN GROUPS OF INDIVIDUALS WITH MCI OR AD COMPARED TO CN.

Group	Label	FA		MD	
		r	p	r	p
CN vs MCI/AD	all	-0.13	**$1.25\times10^{-3*}$**	0.23	**$1.65\times10^{-9*}$**
	core	-0.14	**$4.51\times10^{-4*}$**	0.21	**$4.18\times10^{-8*}$**
	1	-0.03	0.42	0.17	**$9.08\times10^{-6*}$**
	2	-0.08	**0.03**	0.15	**$1.70\times10^{-4*}$**
	3	-0.10	**8.02×10^{-3}**	0.15	**$9.20\times10^{-5*}$**
	4	-0.10	**8.86×10^{-3}**	0.18	**$6.35\times10^{-6*}$**
	5	-0.10	**9.75×10^{-3}**	0.18	**$5.06\times10^{-6*}$**
	6	-0.05	0.23	0.21	**$1.17\times10^{-7*}$**
	7	-0.05	0.22	0.17	**$8.12\times10^{-6*}$**
	8	0.06	0.14	0.14	**$2.21\times10^{-4*}$**
	9	-0.02	0.57	0.12	**$2.31\times10^{-3*}$**
	10	0	0.90	0.11	**$3.52\times10^{-3*}$**
	11	-0.11	**6.68×10^{-3}**	0.17	**$1.09\times10^{-5*}$**
	12	-0.10	**7.49×10^{-3}**	0.18	**$5.92\times10^{-6*}$**
	13	-0.19	**$7.77\times10^{-7*}$**	0.20	**$2.75\times10^{-7*}$**
	14	-0.20	**$4.96\times10^{-7*}$**	0.21	**$9.12\times10^{-8*}$**
	15	-0.14	**$4.75\times10^{-4*}$**	0.22	**$1.50\times10^{-8*}$**

IV. DISCUSSION

We have introduced an along-tract method of population analysis using a new approach we call MeTA. Here, we establish correspondence across subjects while considering differences in the shape of each bundle across subjects using dynamic time warping. We found good, reliable fractional anisotropy (FA) values across 15 segments for MeTA_25% labels in HCP. We further test cross-acquisition protocol compatibility across two very divergent diffusion acquisition schemes in the QTIM dataset, to identify several segments along MeTA_25% for which compatibility can be achieved. This highlights the potential for MeTA in multi-site, multi-study analyses of tractography across diverse acquisition protocols such as those that may be available in large-scale consortia such as ENIGMA [23]. Other methods such as RecoBundles for bundle segmentation, have been shown to be sensitive to the scanner resolution and diffusion-weighted directions [24]. The MeTA approach allows us to capture the regional variation within the bundle at the subject and group levels. Future work will involve analyzing the shape

deviations of each individual segment, and statistical harmonization along tracts for multi-study analyses.

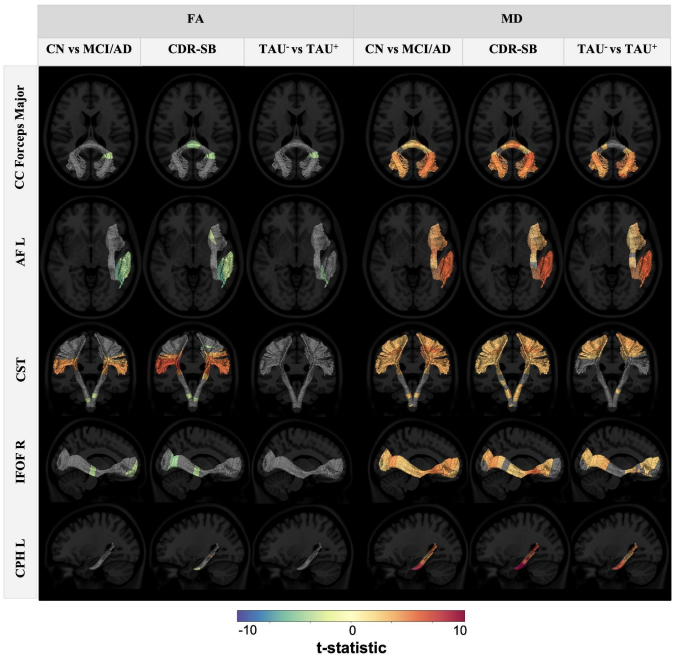

Fig 4. T-values for MeTA_25% along tracts for bundles segmented; colored areas indicate significant associations (P_{FDR}<0.05) with clinical impairment, CDR-SB, and tau pathology.

Acknowledgment

This research was supported by NIH grants P41EB015922, R01AG059874, R01MH134004, and RF1AG057892. Data were provided [in part] by the Human Connectome Project, WU-Minn Consortium (Principal Investigators: David van Essen and Kamil Ugurbil; U54MH091657) funded by the 16 NIH Institutes and Centers that support the NIH Blueprint for Neuroscience Research; and by the McDonnell Center for Systems Neuroscience at Washington University. Alzheimer's Disease Neuroimaging Initiative (ADNI) database (adni.loni.usc.edu). As such, the investigators within the ADNI contributed to the design and implementation of ADNI and/or provided data but did not participate in analysis or writing of this report. A complete listing of ADNI investigators can be found at: http://adni.loni.usc.edu/wp-content/uploads/how_to_apply/ADNI_Acknowledgement_List.pdf.

References

[1] A. Pichet Binette et al., "Bundle-specific associations between white matter microstructure and Aβ and tau pathology in preclinical Alzheimer's disease," Elife, vol. 10, May 2021, doi: 10.7554/eLife.62929.

[2] J. B. Colby, L. Soderberg, C. Lebel, I. D. Dinov, P. M. Thompson, and E. R. Sowell, "Along-tract statistics allow for enhanced tractography analysis," Neuroimage, vol. 59, no. 4, pp. 3227–3242, Feb. 2012.

[3] E. Garyfallidis, M. Brett, M. M. Correia, G. B. Williams, and I. Nimmo-Smith, "QuickBundles, a method for tractography simplification," Front. Neurosci., vol. 6, p. 175, Dec. 2012.

[4] B. Q. Chandio et al., "Bundle analytics, a computational framework for investigating the shapes and profiles of brain pathways across populations," Sci. Rep., vol. 10, no. 1, p. 17149, Oct. 2020.

[5] S. St-Jean, M. Chamberland, M. A. Viergever, and A. Leemans, "Reducing variability in along-tract analysis with diffusion profile realignment," Neuroimage, vol. 199, pp. 663–679, Oct. 2019.

[6] I. Ba Gari et al., "Medial Tractography Analysis (MeTA) for white matter population analyses across datasets," in 2023 11th International IEEE/EMBS Conference on Neural Engineering (NER), Apr. 2023, pp. 1–5.

[7] P. A. Yushkevich, H. Zhang, and J. C. Gee, "Continuous medial representation for anatomical structures," IEEE Trans. Med. Imaging, vol. 25, no. 12, pp. 1547–1564, Dec. 2006.

[8] E. Garyfallidis et al., "Recognition of white matter bundles using local and global streamline-based registration and clustering," Neuroimage, vol. 170, pp. 283–295, Apr. 2018.

[9] D. C. Van Essen et al., "The WU-Minn Human Connectome Project: an overview," Neuroimage, vol. 80, pp. 62–79, Oct. 2013.

[10] N. Jahanshad et al., "Diffusion imaging protocol effects on genetic associations," Proc. IEEE Int. Symp. Biomed. Imaging, pp. 944–947, 2012.

[11] A. Zavaliangos-Petropulu et al., "Diffusion MRI indices and their relation to cognitive impairment in brain aging: The updated multi-protocol approach in ADNI3," Front. Neuroinform., vol. 13, p. 2, Feb. 2019.

[12] C. Sullivan and A. Kaszynski, "PyVista: 3D plotting and mesh analysis through a streamlined interface for the Visualization Toolkit (VTK)," J. Open Source Softw., vol. 4, no. 37, p. 1450, May 2019.

[13] W. Schroeder, K. Martin, and B. Lorensen, The Visualization Toolkit: An object-oriented approach to 3D graphics. Kitware, 2006.

[14] F.-C. Yeh et al., "Population-averaged atlas of the macroscale human structural connectome and its network topology," Neuroimage, vol. 178, pp. 57–68, Sep. 2018.

[15] H. Sakoe and S. Chiba, "Dynamic programming algorithm optimization for spoken word recognition," IEEE Trans. Acoust., vol. 26, no. 1, pp. 43–49, Feb. 1978.

[16] J. V. Manjón, P. Coupé, L. Concha, A. Buades, D. L. Collins, and M. Robles, "Diffusion weighted image denoising using overcomplete local PCA," PLoS One, vol. 8, no. 9, p. e73021, Sep. 2013.

[17] E. Kellner, B. Dhital, V. G. Kiselev, and M. Reisert, "Gibbs-ringing artifact removal based on local subvoxel-shifts," Magn. Reson. Med., vol. 76, no. 5, pp. 1574–1581, Nov. 2016.

[18] J. L. R. Andersson and S. N. Sotiropoulos, "An integrated approach to correction for off-resonance effects and subject movement in diffusion MR imaging," Neuroimage, vol. 125, pp. 1063–1078, Jan. 2016.

[19] B. Jeurissen, J.-D. Tournier, T. Dhollander, A. Connelly, and J. Sijbers, "Multi-tissue constrained spherical deconvolution for improved analysis of multi-shell diffusion MRI data," Neuroimage, vol. 103, pp. 411–426, Dec. 2014.

[20] J. D. Tournier, F. Calamante, A. Connelly, "Improved probabilistic streamlines tractography by 2nd order integration over fibre orientation distributions," in Proceedings of the international society for magnetic resonance in medicine, 2010.

[21] P. E. Shrout and J. L. Fleiss, "Intraclass correlations: uses in assessing rater reliability," Psychol. Bull., vol. 86, no. 2, pp. 420–428, Mar. 1979.

[22] C. R. Jack Jr et al., "Defining imaging biomarker cut points for brain aging and Alzheimer's disease," Alzheimer's. Dement., vol. 13, no. 3, pp. 205–216, Mar. 2017.

[23] P. M. Thompson et al., "ENIGMA and global neuroscience: A decade of large-scale studies of the brain in health and disease across more than 40 countries," Transl. Psychiatry, vol. 10, no. 1, p. 100, Mar. 2020.

[24] K. G. Schilling et al., "Fiber tractography bundle segmentation depends on scanner effects, vendor effects, acquisition resolution, diffusion sampling scheme, diffusion sensitization, and bundle segmentation workflow," Neuroimage, vol. 242, p. 118451, Nov. 2021.